



Open Archive Toulouse Archive Ouverte (OATAO)

OATAO is an open access repository that collects the work of some Toulouse researchers and makes it freely available over the web where possible.

This is an author's version published in: <https://oatao.univ-toulouse.fr/27096>

Official URL : <https://doi.org/10.1109/TAES.2018.2798480>


To cite this version :

Vilà-Valls, Jordi and Closas, Pau and Fernández-Prades, Carles and Curran, James Thomas On the Mitigation of Ionospheric Scintillation in Advanced GNSS Receivers. (2018) IEEE Transactions on Aerospace and Electronic Systems, 54 (4). 1692-1708. ISSN 0018-9251

Any correspondence concerning this service should be sent to the repository administrator:

tech-oatao@listes-diff.inp-toulouse.fr

On the Mitigation of Ionospheric Scintillation in Advanced GNSS Receivers

JORDI VILÀ-VALLS , Senior Member, IEEE
Statistical Inference for Communications and Positioning Department,
Barcelona, Spain

PAU CLOSAS , Senior Member, IEEE
Northeastern University, Boston, MA, USA

CARLES FERNÁNDEZ-PRADES , Senior Member, IEEE
Statistical Inference for Communications and Positioning Department,
Barcelona, Spain

JAMES THOMAS CURRAN , Member, IEEE
European Space Agency, Noordwijk, AG, The Netherlands

Ionospheric scintillation is one of the major threats and most challenging propagation scenarios affecting Global Navigation Satellite Systems (GNSS) and related applications. The fact that this phenomenon causes severe degradations only in equatorial and high latitude regions has led to very few contributions dealing with the fundamental scintillation mitigation problem, being of paramount importance in safety critical applications and advanced integrity receivers. The goal of this paper is twofold, first to bring together the most relevant contributions on GNSS receiver design under scintillation conditions, and then, to propose a new GNSS carrier tracking framework and scintillation mitigation methodology. Scintillation complex gain components are modeled as AR processes and embedded into the state-space formulation, providing the filter the capability to distinguish between dynamics and phase scintillation contributions. In addition, the actual need of robust solutions is solved by using

DOI. No. 10.1109/TAES.2018.2798480

Refereeing of this contribution was handled by J. Morton.

This work was supported by the Spanish Ministry of Economy and Competitiveness through Project TEC2015-69868-C2-2-R (ADVENTURE).

Authors' addresses: J. Vilà-Valls and C. Fernández-Prades are with the Statistical Inference for Communications and Positioning Department, Centre Tecnològic de Telecomunicacions de Catalunya (CTTC/CERCA), Barcelona 08860, Spain, E-mail: (jvila@cttc.cat; cfernandez@cttc.cat); P. Closas is with the Electrical and Computer Engineering Department, Northeastern University, Boston, MA 02115 USA, E-mail: (closas@northeastern.edu); J. T. Curran is with the European Space Agency, Noordwijk 2200, AG, The Netherlands, E-mail: (jamestcurran@ieee.org). (*Corresponding author: Pau Closas.*)

an adaptive filtering approach and directly operating with the baseband received signal. Simulation results, using both synthetic and real scintillation data, are provided to support the theoretical discussion and to show the performance improvements of such new approach.

I. INTRODUCTION

It is well known that drifting ionospheric electron density irregularities may lead to the scintillation of transionospheric radio waves, as in the case of signals broadcast from artificial satellites. Scintillation cannot only degrade signal quality but cause receivers' loss of lock, therefore posing a major threat to Global Navigation Satellite Systems (GNSS) based applications, which demand high levels of accuracy, availability, and integrity. Such effect is particularly intense in equatorial ($\pm 20^\circ$ around the magnetic equator) and polar regions (at auroral latitudes), and in high solar activity events (most scintillation occurs for few hours after sunset on the peak years of the solar cycle), jeopardizing the usage of GNSS technology in critical infrastructures or in applications such as aviation.

Rapid changes in the phase and/or amplitude of a radio signal, in particular deep signal fades caused by ionospheric scintillation, may break a receiver's carrier tracking lock. Phase and amplitude scintillation are intimately related. Rapid phase changes are invariably associated with deep fades. However, some deep fades do not cause rapid phase changes. Since GNSS-based avionics rely on both code and carrier measurements, the loss of carrier tracking lock of a certain satellite channel implies a loss of the corresponding satellite until the carrier tracking lock is re-established, and a prescribed settling period has elapsed. If electron density irregularities cover a large portion of the sky, there is a chance that a receiver may lose more than one satellite simultaneously. Concurrent loss of a significant number of satellites discontinues GNSS navigation. Therefore, strong scintillation could be hazardous in terms of continuity and availability for GNSS and related satellite-based augmentation systems in aviation [1].

Industry trends suggest a move away from primarily code-based positioning and to a direct use of the carrier phase for navigation. This is evidenced by the recent release of a number of real-time-kinematic (RTK) carrier phase positioning receivers by leading mass-market companies [2], [3], targeting low-cost and low-power applications. Moreover, single-frequency precise point positioning (PPP) using mass-market receivers has been possible for some time [4]. Thus, although receiver baseband processing has become resilient to harsh environments, the need for accurate carrier phase measurements means that ionospheric scintillation is a significant challenge.

As a result, there is an increasing interest in the study of this effect. As examples of research activities, we can mention projects such as CIGALA (Concept for Ionospheric Scintillation Mitigation for Professional GNSS in Latin America, [5]), CALIBRA (Countering GNSS high Accuracy applications Limitation due to ionospheric disturbance in BRAzil, [6]), and TRANSMIT (Training Re-

search and Applications Network to Support the Mitigation of Ionospheric Threats, [7]), funded by the European Commission, or MONITOR (MONitoring of the Ionosphere by innovative Techniques, coordinated Observations, and Resources [8]), funded by the European Space Agency. Related to receivers dedicated to ionospheric monitoring, we can mention NovAtel’s GPStation-6 [9], Septentrio’s PolaRxS PRO [10], and TAS-I’s GISMO, involved in the EU FP7 MISW (Mitigation of Space Weather threats to GNSS services [11]).

Synchronization is a key stage in any communication receiver or positioning system, and is typically carried out following a two-state approach: acquisition and tracking. The first stage detects the presence or absence of the desired signal, and in case of positive detection it also provides a coarse estimate of the synchronization parameters (i.e., timing and frequency); the second stage refines those estimates, filtering out noise and tracking any possible time variation [12]. The problem under study concerns the derivation of efficient and robust methods for carrier phase tracking, aiming at ionospheric scintillation mitigation in GNSS. Historically, GNSS receivers used carrier tracking techniques based on well-established phase-locked loop (PLL) and frequency-locked loop (FLL) architectures [13]. In the last decade, the Kalman filter (KF) based solutions have been shown to overcome the limitations of standard architectures, but in their standard form do not provide a solution to the scintillation mitigation problem because of the estimation versus mitigation tradeoff [14].

This paper proposes a new global framework for scintillation mitigation in modern GNSS receivers, providing a comprehensive discussion and generalizing previous results in [14] and [15] with the following main contributions.

- 1) Up-to-date state-of-the-art (SoTA) review on GNSS carrier tracking under ionospheric scintillation.
- 2) A comprehensive analysis of the autoregressive (AR) scintillation approximation, with new results with respect to [14] and [15].
- 3) Generalized state-space formulation taking advantage of the new $\{\text{AR}(q), \text{AR}(p)\}$ scintillation approximation.
- 4) A new robust extended KF (EKF) solution for scintillation mitigation, where in contrast to [14] the filter tracks both phase dynamics, scintillation phase and amplitude, adjusts the AR models’ order together with the filter parameters and system uncertainty, and thus it is able to cope with realistic time-varying propagation conditions.
- 5) The proposed methodology is analyzed via an in-depth simulation analysis, using both synthetic and real scintillation data. Results support the discussion and show the improved accuracy with respect to SoTA techniques.

II. IONOSPHERIC SCINTILLATION MITIGATION AND GNSS CARRIER TRACKING SOTA

This section provides a comprehensive SoTA on GNSS carrier tracking under ionospheric scintillation, covering legacy PLL-based architectures, KF-based approaches, and some alternative multisatellite/multifrequency solutions.

A. Standard PLL-Based Architectures

The earliest contributions dealing with carrier tracking and ionospheric scintillation considered the impact on standard PLL-based architectures. The goal was to find the optimal parameterization to cope with such propagation effects. Different constant bandwidth PLL-based architectures were compared with a KF solution in [16]. The latter provided a lower lock threshold and increased cycle slip robustness due to its optimal time-varying bandwidth. Similar results were shown in [17] and [18]. Even if the KF-based architectures were known to overcome the limitations in the performance and robustness of PLL-type solutions, the latter have been further investigated in the literature. The optimal time-varying KF bandwidth was heuristically implemented using an adaptive bandwidth PLL in [19], also used in [20] together with a scintillation prediction model. An inertially aided F-PLL approach to lower the tracking threshold was proposed in [21] and other Doppler-aiding architectures in [22] and [23]. The traditional F-PLL architecture was analyzed under scintillation conditions in [18], and slightly improved in [24]. A switching PLL/FLL architecture was proposed in [25] and the impact of considering extended integration times for Galileo signals has been recently studied in [26].

B. Advanced KF-Based Solutions

Despite the reluctance of the GNSS community to abandon the use of PLL-based architectures, it is evident that KFs are in the core of the most advanced carrier tracking techniques [27]. Regarding the problem at hand, several contributions followed the initial analysis in [16] and [17]. The use of a suboptimal KF (i.e., not optimally adjusting the Kalman gain) to track both GPS L1 and L2 frequencies under scintillation has been investigated in [28], with the idea to increase robustness using dual-frequency receivers. Other contributions considered the same suboptimal KF implementation with simulated [18], [29], [30] and real data [31], providing an increased robustness with respect to standard PLL-based solutions, even with such a suboptimal filter implementation. The use of more advanced filtering techniques such as particle filters directly operating with the received signal samples has also been considered [32]. The reason why suboptimal KF architectures are considered in the literature instead of the optimal solution is because the latter implies a complete knowledge of the system conditions, that is, process and measurement noise parameters.

The so-called adaptive KFs (AKFs) try to sequentially adapt the filter parameters to the actual working conditions, providing an appealing solution to the previous suboptimal techniques. A global AKF design framework is given in [33]. An heuristic approach to adjust the Kalman gain has been proposed in [34] and a measurement noise adaptation using a C/N_0 estimator was analyzed in [35], a method which was further improved to sequentially adjust both noise statistics [36]. Recently, an ionospheric scintillation monitoring procedure was used to sequentially adjust the process noise covariance together with the C/N_0 estimation

to adjust the measurement noise [37], and further improved to heuristically weight the resulting Kalman gain in [38]. Notice that all these techniques claim robustness against scintillation but none of them provides an effective scintillation mitigation procedure. In other words, the main goal of all the techniques presented in the literature dealing with scintillation is to avoid cycle slips and loss of lock, without paying attention on minimizing the carrier phase estimation error. The robustness is provided by increasing the noise uncertainty under scintillation conditions; for instance, if the C/N_0 drops because of the scintillation, the filter increases the measurement noise variance, thus relies more on the state prediction than on the current measurements. In general, this leads to the estimation versus mitigation tradeoff discussed in [14], impossible to decouple or mitigate such undesired propagation effects if the filter is well designed to keep track under challenging dynamic scenarios (i.e., which is a desirable feature).

From an optimal filtering standpoint, to solve such dilemma one must include the effects to mitigate into the state-space formulation and keep track of both phase contributions. This idea was first introduced in [39] in a quasi-static scenario. These results were generalized to a dynamic case in [14], and a preliminary analysis of a new architecture directly operating with the received signal samples was recently presented in [15]. The goal of this contribution is to generalize all these previous results in an overarching scintillation mitigation framework.

C. Alternative Approaches

All the aforementioned techniques are scalar architectures, that is, considering only a single-frequency, single-satellite link, but other approaches may be envisaged. The fact that ionospheric scintillation is frequency dependent and that different satellite links are definitely affected by different propagation conditions has led to substantial research on multisatellite multifrequency receivers to counteract scintillation effects [40], [41]. The first solutions in this line proposed to modify the position computation by appropriately weighting the pseudorange measurements affected by scintillation [42]–[44], but better performance can be obtained by using the following more sophisticated approaches. Taking advantage of the different satellites available by using vector tracking architectures may lower the tracking threshold and thus increase the robustness and availability under challenging scintillation conditions [40], [45]–[47]. Even if lower frequencies experience a stronger scintillation effect, in the most challenging scenarios (i.e., severe scintillation conditions) the impact of canonical fades in different frequencies have a low correlation [1]. This is the reason why using multifrequency solutions increases the system robustness to scintillation [48]–[50].

Even if the main goal of our contribution is to propose a solution within the scalar tracking framework, the performance obtained with multisatellite, multifrequency approaches could also benefit from the proposed solution.

III. IONOSPHERIC AMPLITUDE AND PHASE SCINTILLATION MODELING

A. Generalities and Scintillation Models

The ionosphere is a region of the upper atmosphere that is ionized by solar radiation. The recombination of waves after propagation through it can be constructive or destructive, and the resulting signal at the receiver antenna may present rapid variations of phase and amplitude. These amplitude fades and phase changes happen in a simultaneous and random manner, but there exists a correlation between both disturbances, the so-called canonical fades. That is, rapid phase changes are always associated with deep amplitude fades [51], [52], which is a very challenging carrier tracking scenario.

A lot of effort has been put in the past two decades to characterize ionospheric scintillation, mainly targeted to obtain effective synthetic models to assess GNSS receivers' performance via simulation. The most widely used ionospheric scintillation models are: WideBand MODEL [53], Global Ionospheric Scintillation Model [54], and Cornell Scintillation Model (CSM) [52], [55]. Among them, the CSM is the more convenient from a simulation point of view and is the one being used throughout this paper.

Related to the mathematical formulation representing the behavior of scintillation onto GNSS signals, the scintillation can be modeled as a multiplicative channel

$$x(t) = \xi_s(t)s(t) + w(t) \quad (1)$$

where $x(t)$ and $s(t)$ are the complex-valued baseband equivalent of the received and transmitted signals, respectively. $w(t)$ is the noise term, which may include thermal noise and any other interference, and the disturbance caused by ionospheric scintillation is defined as

$$\xi_s(t) = \rho_s(t)e^{j\theta_s(t)} \quad (2)$$

with the corresponding envelope and phase components $\rho_s(t)$ and $\theta_s(t)$. The amplitude scintillation strength is described by the scintillation index S_4 , and is usually considered within three main regions [55]: weak, moderate, and severe

$$S_4 = \sqrt{\frac{\mathbb{E}(\rho_s^4) - (\mathbb{E}(\rho_s^2))^2}{(\mathbb{E}(\rho_s^2))^2}}, \quad \begin{cases} S_4 \leq 0.3 & \text{(weak)} \\ 0.3 < S_4 \leq 0.6 & \text{(moderate)} \\ 0.6 < S_4 & \text{(severe)}. \end{cases}$$

B. Ionospheric Scintillation Amplitude AR(q) Model

A key point for the scintillation mitigation problem is to obtain a simple mathematical scintillation approximation, which can be effectively exploited at the receiver side. Preliminary results on the use of an AR model to approximate the correlated scintillation amplitude time series were first introduced in [15], but the modeling was not deeply analyzed and considered only the severe scintillation case with an AR(2) approximation. The general AR(q) model for a discrete sequence $\rho_{s,k}$ is specified by the following

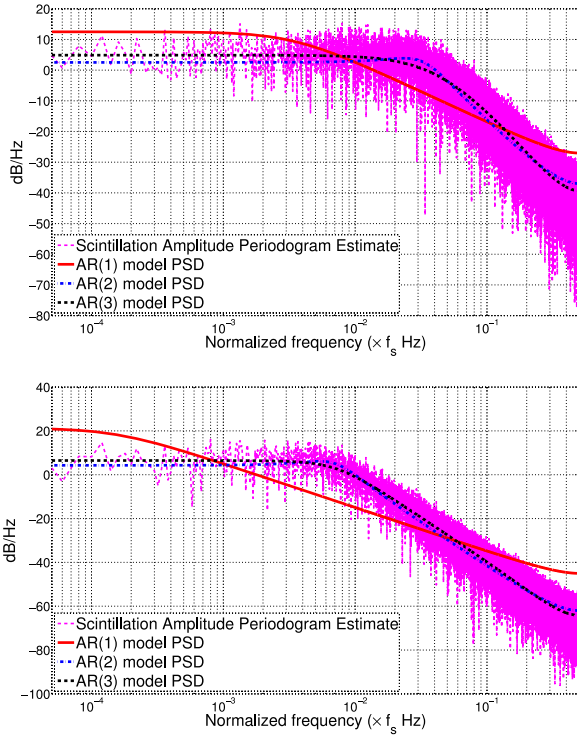


Fig. 1. Scintillation amplitude CSM time-series AR(q) approximation example. Severe (top) $\{S_4 = 0.9, \tau_0 = 0.1\}$ and moderate (bottom) $\{S_4 = 0.5, \tau_0 = 0.4\}$ scintillation amplitude cases.

recursion:

$$\rho_{s,k} = \sum_{i=1}^q \gamma_i \rho_{s,k-i} + \kappa + \eta_{\rho,k}, \quad \eta_{\rho,k} \sim \mathcal{N}(0, \sigma_{\eta_{\rho}}^2) \quad (3)$$

with κ a constant value, and the mean of the process equal to $\mu = \kappa / (1 - \sum_{i=1}^q \gamma_i)$. The set of q coefficients γ_i and the driving noise variance $\sigma_{\eta_{\rho}}^2$ can be easily obtained using time-series analysis [56], for instance, using CSM realistic scintillation amplitude data.

An AR modeling example for the scintillation amplitude is shown in Fig. 1, where both the empirical and fitted AR processes power spectral densities (PSD) are shown for the two main scintillation intensity regions of interest: moderate (bottom figure— $\{S_4 = 0.5, \tau_0 = 0.5\}$) and severe (top figure— $\{S_4 = 0.8, \tau_0 = 0.1\}$) scintillation. These results were computed considering an extended sampling period at the output of the prompt correlator equal to $T_s = 10$ ms, but the same results are also valid for $T_s = 1$ (GPS L1) and 4 ms (Galileo E1) taking into account that a higher T_s increases the scintillation intensity. From a visual inspection of the fitting to the empirical PSD, it is clear that the AR(1) is not valid but it seems that an AR(2) model correctly approximates the scintillation phase amplitude, as already stated in [15]. But to fully characterize such modeling, it is convenient to inspect the partial autocorrelation function (PAF). The PAF for both scintillation cases is shown in Fig. 2, where it is clear that the correct model order is $q = 3$, because the lag 3 value clearly exceeds the 95% confidence bound.

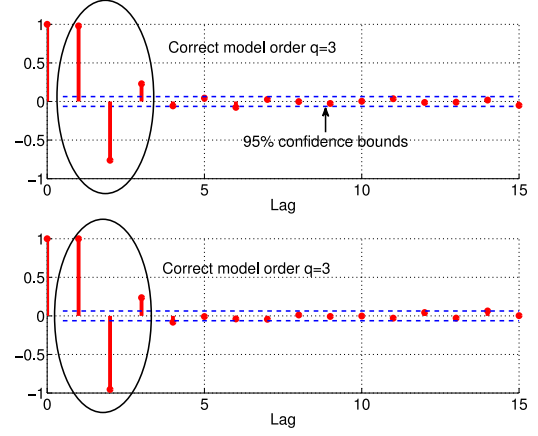


Fig. 2. Sample PAF for model order selection. Severe (top) $\{S_4 = 0.9, \tau_0 = 0.1\}$ and moderate (bottom) $\{S_4 = 0.5, \tau_0 = 0.4\}$ scintillation amplitude cases.

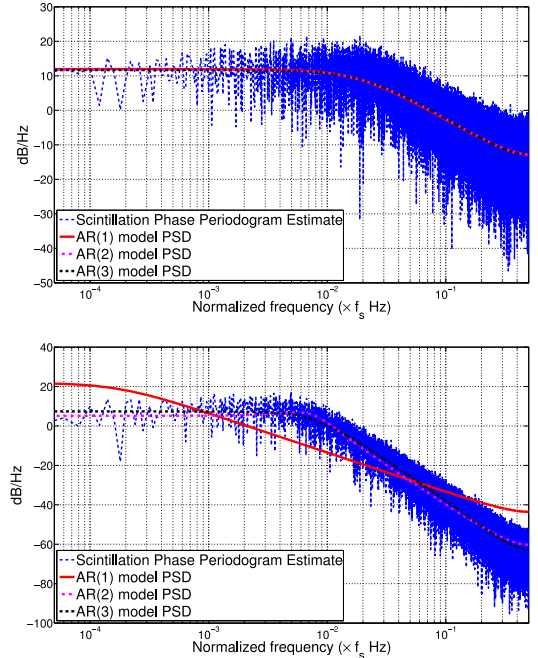


Fig. 3. Scintillation phase CSM time-series AR(p) approximation example. Severe (top) $\{S_4 = 0.9, \tau_0 = 0.1\}$ and moderate (bottom) $\{S_4 = 0.5, \tau_0 = 0.4\}$ scintillation phase cases.

C. Ionospheric Scintillation Phase AR(p) Model

The scintillation amplitude AR modeling analysis conducted in the previous paragraphs may also be applied to the correlated scintillation phase. The use of an AR model for the scintillation phase process was first introduced in [39] and later on analyzed in [14] using a visual inspection of the PSD fitting, but such analysis does not conclude on the correct AR model order selection. The phase AR formulation is

$$\theta_{s,k} = \sum_{i=1}^p \beta_i \theta_{s,k-i} + \eta_{\theta,k}, \quad \eta_{\theta,k} \sim \mathcal{N}(0, \sigma_{\eta_{\theta}}^2). \quad (4)$$

A representative example is given in Fig. 3 considering an extended sampling period $T_s = 10$ ms. As in the

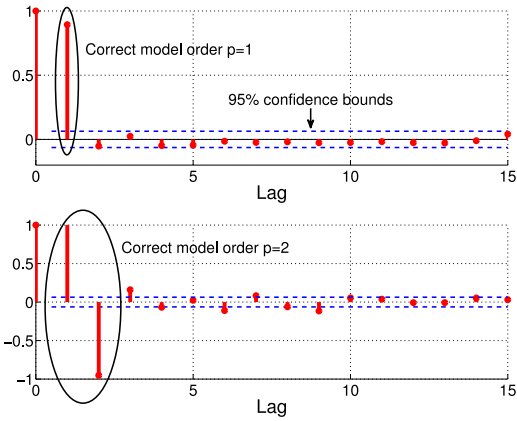


Fig. 4. Sample PAF for model order selection. Severe (top) $\{S_4 = 0.9, \tau_0 = 0.1\}$ and moderate (bottom) $\{S_4 = 0.5, \tau_0 = 0.4\}$ scintillation phase cases.

TABLE I
AR(q) Amplitude and AR(p) Phase
Scintillation Approximation

Scintillation region	AR model order	
	q	p
Severe ($0.6 < S_4$)	AR(3)	AR(1)
Moderate ($0.3 < S_4 \leq 0.6$)	AR(3)	AR(2)
Low ($S_4 \leq 0.3$)	AR(3)	AR(3)

scintillation amplitude case shown in Fig. 1, these results are also valid for $T_s = 1$ (GPS L1) and 4 ms (Galileo E1).

The correct model order selection is verified from further analysis conducted using the PAF, as shown in Fig. 4. To conclude, we summarize in Table I the $\{AR(q), AR(p)\}$ scintillation approximation.

IV. SIGNAL MODEL

A. GNSS Signal Model

The baseband analytic representation of a generic GNSS transmitted signal can be expressed as

$$s(t) = \sqrt{2P_x(t)}d(t - \tau(t))c(t - \tau(t))e^{j\theta(t)} \quad (5)$$

where $P_x(t)$, $d(t)$, and $c(t)$ stand for the received power, the navigation message, and the spreading code, respectively. The synchronization parameters are the code delay $\tau(t)$ and the carrier phase $\theta(t)$. The latter can be formulated as $\theta(t) = 2\pi f_d(t) + \theta_e(t)$, where $f_d(t)$ is the carrier Doppler frequency shift and $\theta_e(t)$ a carrier phase component including other phase impairments. After the acquisition stage, the sampled signal is correlated with a locally generated replica and then accumulated over the integration period T_s . The samples at the output of the correlators are [57]

$$y_k = A_k d_k R(\Delta\tau_k) \frac{\sin(\pi \Delta f_{d,k} T_s)}{\pi \Delta f_{d,k} T_s} e^{j(2\pi \Delta f_{d,k} T_s + \Delta\theta_k)} + n_k$$

where k stands for the discrete time $t_k = kT_s$, A_k is the signal amplitude at the output of the correlators after accumulation over T_s , d_k is the data bit, $R(\cdot)$ is the code autocorrelation function, and $\{\Delta\tau_k, \Delta f_{d,k}, \Delta\theta_k\}$ are, respectively, the code delay, Doppler shift, and carrier phase errors. The noise at the output of the correlators is considered additive complex Gaussian with variance $\sigma_{n,k}^2$, that is, $n_k \sim \mathcal{CN}(0, \sigma_{n,k}^2)$. Taking into account the problem at hand, a simplified signal model with perfect timing synchronization ($\Delta\tau_k = 0$) and data wipe-off can be considered. Under these assumptions, the simplified model for the samples at the input of the carrier phase tracking stage is $y_k = \alpha_k e^{j\theta_k} + n_k$, or equivalently

$$\begin{bmatrix} y_{i,k} \\ y_{q,k} \end{bmatrix} = \alpha_k \begin{bmatrix} \cos(\theta_k) \\ \sin(\theta_k) \end{bmatrix} + \begin{bmatrix} n_{i,k} \\ n_{q,k} \end{bmatrix} \quad (6)$$

where $y_k = y_{i,k} + iy_{q,k}$ and $n_k = n_{i,k} + in_{q,k}$, with covariance matrix $\mathbf{R}_k = \sigma_{n,k}^2/2 \times \mathbf{I}_2$; the amplitude α_k may include the scintillation variations, $\alpha_k = A_k \rho_{s,k}$; and the carrier phase includes both the phase variations due to the receiver's dynamics $\theta_{d,k}$ and scintillation $\theta_{s,k}$, resulting in $\theta_k = \theta_{d,k} + \theta_{s,k}$. This is the equivalent signal model at the output of the prompt correlator considering the multiplicative channel model. The signal amplitude under nominal propagation conditions A_k can be easily estimated using a maximum-likelihood approach [58] or assuming nominal noise power from the C/N_0 and the receiver bandwidth [13]. This amplitude varies very slowly w.r.t. the periods when the signal is affected by scintillation, thus the nominal estimated value can be used.

B. New Generalized State-Space Formulation

The state-space formulation of the problem is given by a pair of equations, which define the state evolution (process equation) and its relation with the observations (measurement equation). Taking into account the problem at hand, the parameter of interest is the received signal carrier phase θ_k . As already stated, in real-life applications this phase may encompass different contributions, but only the phase variations due to the relative movement between the satellite and the receiver $\theta_{d,k}$ are modeled in standard architectures. In this case, a Taylor approximation of the time-varying phase evolution is considered, where the order m is *a priori* determined according to the expected dynamics (i.e., $2 \leq m \leq 4$ in standard applications). The fourth-order Taylor expansion is given by

$$\theta_{d,k} = \theta_0 + 2\pi \left(f_{d,k} k T_s + \underbrace{f_{r,k} k^2 T_s^2 / 2 + f_{j,k} k^3 T_s^3 / 6}_{\text{Doppler dynamics}} \right) \quad (7)$$

where θ_0 (rad) is a random constant phase value, $f_{d,k}$ (Hz) the carrier Doppler frequency shift, $f_{r,k}$ (Hz/s) the Doppler frequency rate, and $f_{j,k}$ (Hz/s²) the Doppler jerk. Using this approximation, the state to be tracked is $\mathbf{x}_k^{(1)} \doteq [\theta_{d,k} \ f_{d,k} \ f_{r,k} \ f_{j,k}]^\top$, and the standard carrier phase

state evolution equation is formulated as

$$\mathbf{x}_k^{(1)} = \underbrace{\begin{pmatrix} 1 & 2\pi T_s & \pi T_s^2 & \pi T_s^3/6 \\ 0 & 1 & T_s & T_s^2/2 \\ 0 & 0 & 1 & T_s \\ 0 & 0 & 0 & 1 \end{pmatrix}}_{\mathbf{F}_d} \mathbf{x}_{k-1}^{(1)} + \mathbf{v}_k \quad (8)$$

where $\mathbf{v}_k \sim \mathcal{N}(0, \mathbf{Q}_{d,k})$ stands for possible uncertainties or mismatches on the dynamic model, and $\mathbf{Q}_{d,k}$ is usually *a priori* fixed according to the problem at hand. An extended state space can be formulated to include the scintillation phase [14], [39] or both scintillation amplitude and phase [15], but taking advantage of the new generalized $\{\text{AR}(p), \text{AR}(q)\}$ models introduced in the previous section

$$\begin{aligned} \theta_{s,k} &= \sum_{i=1}^p \beta_i \theta_{s,k-i} + \eta_{\theta,k}, \quad \eta_{\theta,k} \sim \mathcal{N}(0, \sigma_{\eta_{\theta}}^2) \quad (9) \\ \rho_{s,k} &= \sum_{i=1}^q \gamma_i \rho_{s,k-i} + \kappa + \eta_{\rho,k}, \quad \eta_{\rho,k} \sim \mathcal{N}(0, \sigma_{\eta_{\rho}}^2). \end{aligned} \quad (10)$$

The extended state is constructed by concatenating the standard formulation and the new scintillation modeling, $\mathbf{x}_k^{(2)} \doteq [\mathbf{x}_k^{(1)}, \theta_{s,k}, \dots, \theta_{s,k-p+1}, \rho_{s,k}, \dots, \rho_{s,k-q+1}]^\top$, and the corresponding process equation is

$$\mathbf{x}_k^{(2)} = \underbrace{\begin{pmatrix} \mathbf{F}_d & \mathbf{0}_{m \times p} & \mathbf{0}_{m \times q} \\ \mathbf{0}_{p \times m} & \mathbf{F}_p & \mathbf{0}_{p \times q} \\ \mathbf{0}_{q \times m} & \mathbf{0}_{q \times p} & \mathbf{F}_a \end{pmatrix}}_{\mathbf{F}_k} \mathbf{x}_{k-1}^{(2)} + \boldsymbol{\kappa} + \mathbf{w}_k \quad (11)$$

where the Gaussian process noise is defined as $\mathbf{w}_k = [\mathbf{v}_k, \eta_{ph,k}, \mathbf{0}_{1 \times p-1}, \eta_{a,k}, \mathbf{0}_{1 \times q-1}]^\top$, with a block-diagonal covariance matrix $\mathbf{Q}_k = \text{diag}(\mathbf{Q}_{d,k}, \sigma_{\eta_{\theta}}^2, \mathbf{0}_{1 \times p-1}, \sigma_{\eta_{\rho}}^2, \mathbf{0}_{1 \times q-1})$, and the scintillation transition matrices are

$$\mathbf{F}_p = \begin{pmatrix} \beta_1 & \beta_2 & \dots & \beta_p \\ 1 & & & \\ & \ddots & & \\ & & & 1 \end{pmatrix}, \quad \mathbf{F}_a = \begin{pmatrix} \gamma_1 & \gamma_2 & \dots & \gamma_q \\ 1 & & & \\ & \ddots & & \\ & & & 1 \end{pmatrix}.$$

Equations (6) and (11) define the new state-space model (SSM) of the problem, allowing the filter to be aware of both phase contributions, together with the signal fading caused by the scintillation, being much more powerful than its standard version only taking into account the dynamics $\theta_{d,k}$.

V. GNSS CARRIER TRACKING TECHNIQUES UNDER IONOSPHERIC SCINTILLATION

The carrier synchronization problem under study consists of obtaining the best estimate of the phase related to the user dynamics $\theta_{d,k}$. This implies the mitigation of the ionospheric scintillation of interest here.

A. Traditional PLL and KF-Based Tracking Techniques

Carrier phase tracking techniques used in mass-market GNSS receivers typically rely on well-established PLL-based architectures [13], which are built up using a phase detector (referred to as *discriminator* in this context), a filter, and a carrier generator driven by a numerically controlled oscillator. Such architecture is easy to implement and tune, and provides good performances under benign propagation conditions, but has been shown to deliver poor performance or even fail in challenging scenarios [18]. The main problem is the existing noise reduction versus dynamic range tradeoff [34], mainly driven by the PLL constant bandwidth. The PLL minimizes the error signal at the discriminator's output, $\epsilon_k = \theta_k - \hat{\theta}_k$, and thus the filter tracks the complete phase of the signal. This implies that, under scintillation conditions, the PLL will track the desired phase plus scintillation disturbance, $\theta_k = \theta_{d,k} + \theta_{s,k}$, what is known as the estimation versus mitigation paradigm [14]. As a consequence, a well-designed PLL is not able to mitigate the scintillation effect.

It is well known that, under certain conditions, both PLL and KF architectures are equivalent [59]–[61]. The standard prediction/update KF equations [62] can be easily interpreted as a gain PLL [61], where the KF innovations' sequence can be seen as the output of a discriminator. The standard KF formulation, as implicitly done by the PLL, considers that $\theta_k = \theta_{d,k}$. Therefore, the filter is again constrained by the system model and not able to mitigate the undesired scintillation effects. The phase noise variance at the discriminators' output, which is needed in the linear KF to compute the Kalman gain, is no longer σ_n^2 . An approximation of the phase noise variance for the ATAN discriminator is given by [63]

$$\sigma_{n_{\theta}}^2 \approx \frac{(e^{-0.8\sqrt{C/N_0 T_s}} + 1) \text{erf}(0.4C/N_0 T_s)}{C/N_0 T_s} \quad (12)$$

where C/N_0 stands for the carrier-to-noise-density ratio.

In standard GNSS receivers, a C/N_0 estimator is generally available, from which a sequential phase noise estimate can be derived via (12), making it straightforward to construct an AKF [64]. In summary, standard PLL and KF-based techniques track the complete phase of the incoming signal θ_k , and therefore it is difficult to decouple both phase contributions to mitigate such undesired effects.

B. New Scintillation Mitigation Methodology

The new state-space formulation including both dynamics, scintillation amplitude fades, and phase contributions, needed to solve the scintillation mitigation problem, is detailed in Section IV-B and given by the state $\mathbf{x}_k^{(2)}$ and observations $[y_{i,k}, y_{q,k}]^\top$ in (6) and (11). The SSM is fully characterized by the set of parameters $\{m, p, q, \{\beta_i\}_{i=1}^p, \{\gamma_i\}_{i=1}^q, \kappa, \sigma_{\eta_{\theta}}^2, \sigma_{\eta_{\rho}}^2, \mathbf{Q}_{d,k}, \sigma_{n,k}^2\}$, and their values can be set according to the following criteria.

- 1) m and $\mathbf{Q}_{d,k}$ are *a priori* fixed by the user from the expected dynamics (typically, $m = 3$).

- 2) The AR scintillation model orders p and q are directly related to the scintillation intensity (see Table I).
- 3) $\{\beta_i\}_{i=1}^p, \{\gamma_i\}_{i=1}^q, \kappa, \sigma_{\eta_\theta}^2$, and $\sigma_{\eta_\rho}^2$ are the parameters of the $\{\text{AR}(q), \text{AR}(p)\}$ scintillation model approximation, which can be computed offline from the CSM time series or the simulation of choice for a known scintillation intensity, and easily stored in a look-up table.
- 4) $\sigma_{n,k}^2$ can be sequentially estimated from the C/N_0 estimator available at the receiver [64].

In general, at the light of Table I, four SSMs are distinguished depending on the scintillation propagation conditions (i.e., for an *a priori* fixed $m = 3$ and $\mathbf{x}_k^{(1)} = [\theta_{d,k}, f_{d,k}, f_{r,k}]$).

- 1) SSM #1: No scintillation—The state to be tracked is $\mathbf{x}_k^{(1)}$.
- 2) SSM #2: Severe scintillation—The state to be tracked is

$$\mathbf{x}_k^{(2)} = \left[\mathbf{x}_k^{(1)}, \underbrace{\theta_{s,k}}_{p=1}, \underbrace{\rho_{s,k}, \rho_{s,k-1}, \rho_{s,k-2}}_{q=3} \right]^\top$$

where $\{\beta_1, \gamma_1, \gamma_2, \gamma_3, \kappa, \sigma_{\eta_\theta}^2, \sigma_{\eta_\rho}^2\}$ is the set of parameters that fully characterize the severe scintillation AR(1)/AR(3) approximation.

- 3) SSM #3: Moderate scintillation—The state is defined as

$$\mathbf{x}_k^{(2)} = \left[\mathbf{x}_k^{(1)}, \underbrace{\theta_{s,k}, \theta_{s,k-1}}_{p=2}, \underbrace{\rho_{s,k}, \rho_{s,k-1}, \rho_{s,k-2}}_{q=3} \right]^\top$$

where $\{\beta_1, \beta_2, \gamma_1, \gamma_2, \gamma_3, \kappa, \sigma_{\eta_\theta}^2, \sigma_{\eta_\rho}^2\}$ is the set of parameters that fully characterize the moderate scintillation AR(2)/AR(3) approximation.

- 4) SSM #4: Low scintillation—The state to be tracked is defined as

$$\mathbf{x}_k^{(2)} = \left[\mathbf{x}_k^{(1)}, \underbrace{\theta_{s,k}, \theta_{s,k-1}, \theta_{s,k-2}}_{p=3}, \underbrace{\rho_{s,k}, \rho_{s,k-1}, \rho_{s,k-2}}_{q=3} \right]^\top$$

where $\{\beta_1, \beta_2, \beta_3, \gamma_1, \gamma_2, \gamma_3, \kappa, \sigma_{\eta_\theta}^2, \sigma_{\eta_\rho}^2\}$ is the set of parameters that fully characterize the low scintillation AR(3)/AR(3) approximation.

A standard discriminator-based KF can be easily constructed for one of the SSMs following the architecture introduced in Section V-A. But such architecture lacks robustness and adaptivity, and is not suited for time-varying scintillation conditions. Instead of using a discriminator-based approach, as previously done in [14], this paper proposes an EKF directly operating with the received signal

complex samples. Such approach avoids the discriminator's nonlinearities and possible saturation at low C/N_0 , resulting in a more robust architecture. The main idea behind the EKF consists of linearizing the possibly nonlinear process and measurement functions around the predicted and updated state estimates, and then applying the standard linear KF equations [62]. In this case, only the measurement equation is nonlinear and reads

$$\mathbf{h}_k(\mathbf{x}_k^{(2)}) = A_k \rho_{s,k} \begin{bmatrix} \cos(\theta_{d,k} + \theta_{s,k}) \\ \sin(\theta_{d,k} + \theta_{s,k}) \end{bmatrix}. \quad (13)$$

The linearized measurement matrix is given in (14) shown at the bottom of this page, for the SSM #4 case (i.e., AR(3)/AR(3) approximation). This matrix is used in the measurement update step of the EKF, computed¹ as $\tilde{\mathbf{H}}_k = \nabla \mathbf{h}_k(\mathbf{x}_k^{(2)})$ and evaluated at $\mathbf{x}_k^{(2)} = \hat{\mathbf{x}}_{k|k-1}$ (i.e., note that $\hat{\theta}_{k|k-1} \doteq \hat{\theta}_{d,k|k-1} + \hat{\theta}_{s,k|k-1}$). Notice that the state prediction under strong scintillation events may be inaccurate, but the filter takes this naturally into account in the update step via the innovation sequence.

The knowledge of the scintillation intensity is an important point in the system model formulation and SSM parameterization. The possible ionospheric scintillation affecting the system is in general unknown and time varying, but it has been shown in the literature that the time-varying scintillation intensity $S_{4,k}$ may be correctly estimated from the incoming signal [65]. Such estimator can be considered as a scintillation detector and can be used to fix the AR model order parameters q and p , and sequentially update the AR models parameters. Taking into account that different SSMs have different dimensions, the first approach is to use a bank of four parallel EKFs, one for each SSM, together with a scintillation indicator to decide the final estimate at every time instant. This scheme is not convenient because it is computationally inefficient, suboptimal, and may lead to divergence. A second option is to use a more sophisticated single filter architecture, which must be properly designed to cope with such multiple SSM scenario. This solution is more robust and optimal from an estimation point of view, being the preferred architecture in this contribution.

A key point on the filter design is to realize that the state formulation of SSMs #1–#3 can be seen as a subset of the state in SSM #4. Therefore, with a proper parameterization of $\{\beta_1, \beta_2, \beta_3, \gamma_1, \gamma_2, \gamma_3, \kappa, \sigma_{\eta_{ph}}^2, \sigma_{\eta_a}^2\}$, which may be considered time varying, SSM #4 turns to be equivalent to SSMs #1–#3 (e.g., if $\beta_2 = \beta_3 = 0$, SSM #4 \rightarrow SSM #2). This SSM modulation is done via the time-varying state transition matrix $\mathbf{F}_k(S_{4,k})$, which depends on the

¹The vector differential operator is defined as $\nabla = \left[\frac{\partial}{\partial x_1}, \dots, \frac{\partial}{\partial x_n} \right]$.

$$\tilde{\mathbf{H}}_k = \begin{bmatrix} -A_k \hat{\rho}_{s,k|k-1} \sin(\hat{\theta}_{k|k-1}) & 0 & 0 & -A_k \hat{\rho}_{s,k|k-1} \sin(\hat{\theta}_{k|k-1}) & 0 & 0 & A_k \cos(\hat{\theta}_{k|k-1}) & 0 & 0 \\ A_k \hat{\rho}_{s,k|k-1} \cos(\hat{\theta}_{k|k-1}) & 0 & 0 & A_k \hat{\rho}_{s,k|k-1} \cos(\hat{\theta}_{k|k-1}) & 0 & 0 & A_k \sin(\hat{\theta}_{k|k-1}) & 0 & 0 \end{bmatrix}. \quad (14)$$

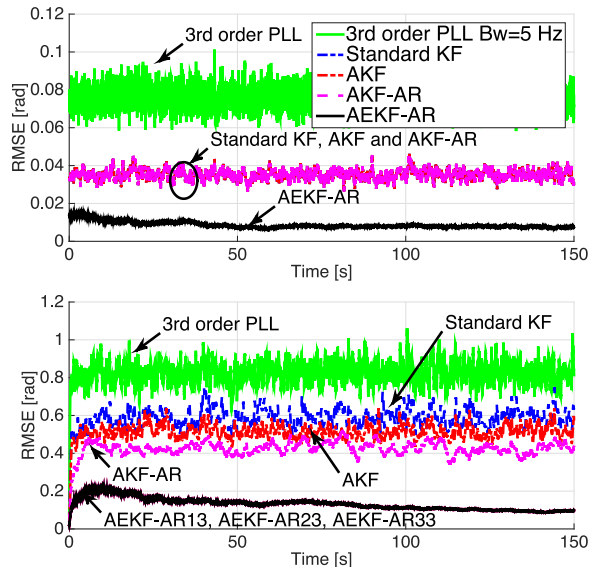


Fig. 6. (Top) RMSE obtained with the proposed AEKF-AR and the SoTA techniques for a scintillation-free standard scenario. (Bottom) RMSE obtained with different methods specified in Table II for a severe scintillation ($S_4 = 0.8$ and $\tau_0 = 0.2$) propagation scenario.

TABLE II
Specification of the Different Methods Used to Validate the Equivalence Between SSMs #2-#4

Name	AR(p)-AR(q)	SSM	AR(p) parameters
AEKF-AR13	AR(1)-AR(3)	SSM #2	$\beta_1 \neq 0$
AEKF-AR23	AR(2)-AR(3)	SSM #3	$\beta_1 \neq 0, \beta_2 = 0$
AEKF-AR33	AR(3)-AR(3)	SSM #4	$\beta_1 \neq 0, \beta_2 = \beta_3 = 0$

different EKF-based solutions, which are sketched in Table II, is given in Fig. 6 (bottom) for a severe scintillation propagation scenario. In this case, it was shown that an AR(1) correctly fits the scintillation phase (SSM #2), thus the validation test considers an AR(2) with $\beta_2 = 0$ (SSM #3) and an AR(3) with $\beta_2 = \beta_3 = 0$ (SSM #4). The performances obtained with the different configurations are equal, thus the architectures are equivalent. The performance obtained with the rest of the techniques is shown for completeness.

B. Case II: Steady-State Performance

In synchronization systems, the steady-state RMSE is an important and statistically significant performance measure. The impact of the ionospheric scintillation into the received signal mainly depends on the scintillation intensity, being of interest in this study the moderate and severe/extreme intensity regions (i.e., the impact of weak scintillation is marginal).

1) *Severe Scintillation*: This may be considered one of the most challenging GNSS carrier tracking scenarios, because these are the conditions that lead to the so-called canonical fades [51], that is, large amplitude fades associated with half-cycle phase jumps. In terms of tracking performance and scintillation mitigation, this is the most representative case to show the potential of the proposed new

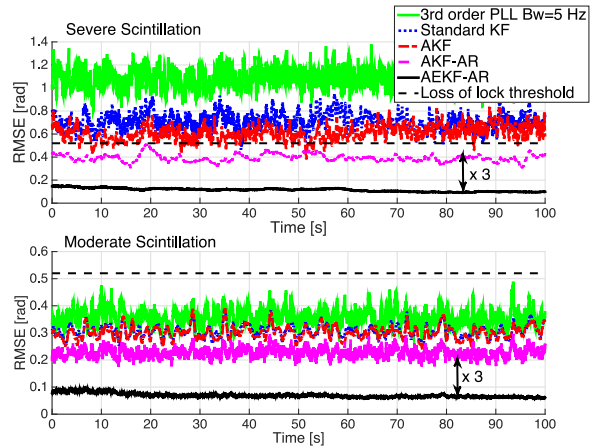


Fig. 7. RMSE obtained for an extreme scintillation propagation scenario, $S_4 = 0.9$ and $\tau_0 = 0.1$ (top), and a moderate scintillation case, $S_4 = 0.5$ and $\tau_0 = 0.4$ (bottom).

TABLE III
Steady-State RMSE [rad] Performance for the Different Methods in Several Scintillation Scenarios

Scintillation	PLL	KF	AKF	AKF-AR	AEKF-AR
$S_4 = 0.9, \tau_0 = 0.1$	1.1	0.71	0.61	0.43	0.12
$S_4 = 0.8, \tau_0 = 0.2$	0.83	0.59	0.52	0.42	0.10
$S_4 = 0.7, \tau_0 = 0.3$	0.63	0.49	0.48	0.42	0.10
$S_4 = 0.6, \tau_0 = 0.4$	0.47	0.40	0.39	0.29	0.08
$S_4 = 0.5, \tau_0 = 0.4$	0.36	0.31	0.30	0.23	0.07
$S_4 = 0.4, \tau_0 = 0.8$	0.26	0.25	0.25	0.20	0.07

architecture. The steady-state performance results obtained for an extreme scintillation case, $S_4 = 0.9$ and $\tau_0 = 0.1$, are shown in Fig. 7 (top), where the performance improvement with respect to both SoTA techniques and the AKF-AR becomes clear.

In GNSS receivers, the loss of lock rule of thumb for the standard deviation is usually fixed to $\sigma = 0.52$ rad (i.e., $3\sigma = 90^\circ$) [13]. Therefore, while legacy techniques (PLL, KF, and AKF) are out of the lock region, only the methods including the scintillation AR modeling into the state space provide good performances. Notice that the RMSE obtained with the new architectures is three times lower than the AKF-AR previously introduced in [14]. These results show the superior performance gain provided by the new approach.

2) *Moderate Scintillation*: A representative example of the steady-state RMSE performance obtained in the moderate region ($S_4 = 0.5$ and $\tau_0 = 0.4$) is shown in Fig. 7 (bottom). In this case, the impact of the scintillation is lower compared to the previous one, and all the methods are below the loss of lock threshold, but the performance obtained with the new AEKF-AR is still three times better than with the AKF-AR, and up to five times better than with the standard techniques.

For the sake of completeness, Table III shows the RMSE (in radians) obtained in several scintillation scenarios. Several conclusions can be obtained from these results, which are as follows.

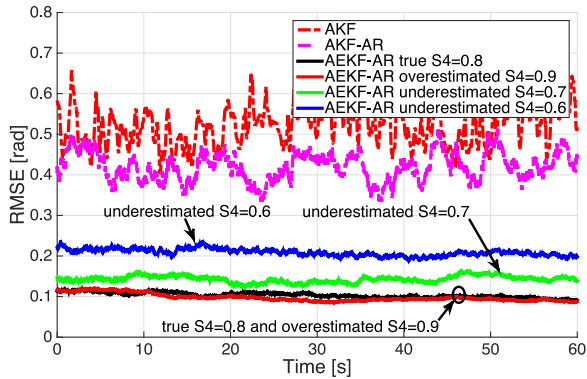


Fig. 8. RMSE considering a correct scintillation AR fit ($S_4 = 0.8$) and several AEKF-AR with an AR modeling mismatches [overestimation ($S_4 = 0.9$) and underestimating ($S_4 = 0.7, 0.6$)].

- 1) The AEKF-AR is always far beyond in terms of tracking performance and scintillation mitigation capabilities.
- 2) The AKF-AR [14] provides slightly better performances than standard techniques, but has been clearly outperformed by the new EKF-based solution.
- 3) Standard techniques are out of the lock region in severe scintillation conditions, where only the new approach is an acceptable solution in terms of integrity.

C. Case III: Robustness to Modeling Mismatch

To fully characterize the new architecture, it is of capital importance to assess its robustness to AR modeling mismatches. In other words, if the scintillation prediction method is inaccurate, the SSM parameters $\{\{\beta_i\}_{i=1}^p, \{\gamma_i\}_{i=1}^q, \kappa, \sigma_{\eta_{ph}}^2, \sigma_{\eta_a}^2\}$ will deviate from the best fit, then the performance obtained with the AEKF-AR may be lower. The question is how much do we lose? Two cases may be considered: the predicted scintillation intensity is higher (i.e., scintillation overestimation), or lower (i.e., scintillation underestimation) than the true one.

Fig. 8 shows the performance obtained for different AR modeling mismatches in a severe scintillation case ($S_4 = 0.8$ and $\tau_0 = 0.2$), being again the most challenging scenario. It is important to see that considering an overestimation of the scintillation intensity has no impact on the receiver performance, while considering lower intensities slightly degrades the tracking results. From these results, it is clear that the new method is robust to modeling mismatches, because even if the filter performance underestimating the scintillation intensity is slightly lower, it is still much better than with the standard techniques and the AKF-AR. From the complimentary RMSE results shown in Table IV, notice that for a moderate scintillation scenario the impact of the AR modeling mismatch is marginal, what supports the robustness of the method.

D. Case IV: Adaptivity to Time-Varying Conditions

To conclude the performance analysis using realistic synthetic data, the last missing point is to assess the adaptivity of the new architecture, that is, how it behaves in time-

TABLE IV
AEKF-AR Steady-State RMSE [Rad] Performance Considering a Scintillation AR Modeling Mismatch

Predicted scintillation	True scintillation $S_4 = 0.8$	True scintillation $S_4 = 0.6$
$S_4 = 0.9, \tau_0 = 0.1$	0.102	–
$S_4 = 0.8, \tau_0 = 0.2$	0.10	0.0802
$S_4 = 0.7, \tau_0 = 0.3$	0.1512	0.0832
$S_4 = 0.6, \tau_0 = 0.4$	0.21	0.078
$S_4 = 0.5, \tau_0 = 0.4$	–	0.0828
$S_4 = 0.4, \tau_0 = 0.8$	–	0.0829

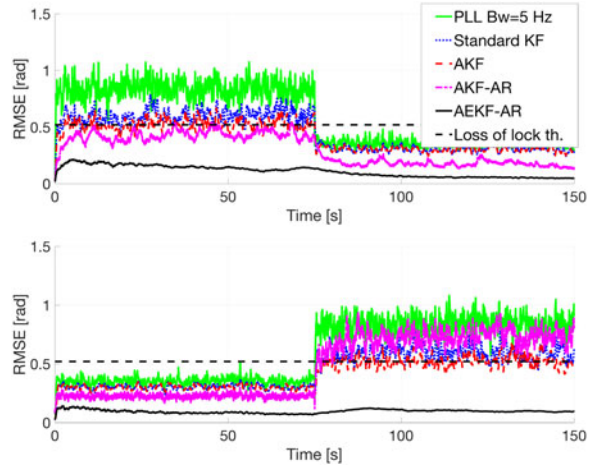


Fig. 9. RMSE considering time-varying scintillation conditions. Severe ($S_4 = 0.8$ and $\tau_0 = 0.2$) to moderate ($S_4 = 0.5$ and $\tau_0 = 0.4$) scintillation transition (top) and vice versa (bottom).

varying scintillation conditions. Two scenarios are considered: a change from severe to moderate scintillation and a change from moderate to severe scintillation. Notice that the transition between scintillation regions is not smooth as it would be in real life, but it is sought to be like this to really assess the method's sensitivity and the performance limits to such harsh propagation conditions.

The results obtained in both time-varying cases are shown in Fig. 9. The top plot shows the performance obtained in the first case, that is, a severe ($S_4 = 0.8$ and $\tau_0 = 0.2$) to moderate ($S_4 = 0.5$ and $\tau_0 = 0.4$) scintillation transition. The AEKF-AR clearly adapts the parameters to the scintillation conditions and provides a good performance. The bottom plot shows the counterpart example, with a transition from moderate scintillation to severe conditions. Again the AEKF-AR provides a robust solution, and the filter keeps the performance in the severe scintillation region as low as in the moderate conditions. In this case the AKF-AR [14], which does not adapt the filter parameters to time-varying conditions, does not provide a good result under severe conditions because the filter is tuned to fit the moderate scintillation. The overall results confirm the good behavior, adaptability, and robustness of the proposed AEKF-AR in front of the rest of the standard methods.

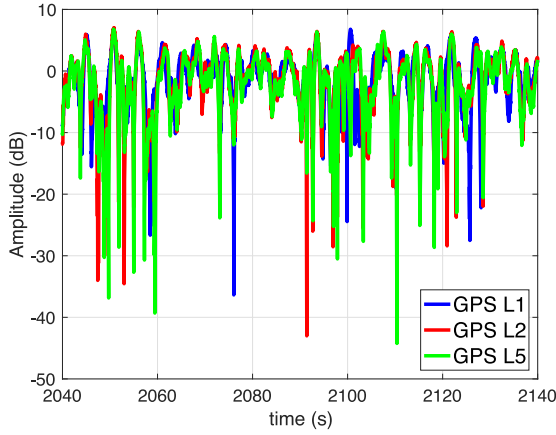


Fig. 10. An example of 100 s of real scintillation amplitude data for the strong scintillation event #1 at three different GPS frequency bands.

E. Case V: Real GPS Scintillation Data

Finally, in this section, we analyze the performance of the new adaptive EKF-AR tracking methodology using real scintillation data, and verify the correct behavior of the AR scintillation modeling with the comparison of amplitude/phase scintillation tracking performances at three GPS frequency bands for different scintillation events. In this case, the RMSE refers to the mean error over the processed sequence.

1) *Real Scintillation Data*: We obtained from the Joint Research Centre (JRC) Scintillation Repository, a collection of data with more than 10 h of scintillation events recorded over Hanoi in March and April, 2015 [66]. These receivers were based on a reconfigurable quad-channel front end (stationary platform), Fortune, which was configured to collect L1, L2, and L5, using 1-b complex sampling at rates of 5, 5, and 30 MHz, respectively [66]. The front end was configured to continuously record 50-min datasets and to postprocess each using an L1 software defined receiver for the purposes of basic scintillation detection. Those datasets in which severe scintillation was identified were then archived for postprocessing, and the others discarded [67].

The postprocessing stage employed a multifrequency open-loop software receiver, which exploited precise knowledge of the receiver location, and the well-disciplined reference oscillator to generate accurate reference carrier and code local replicas. Once demodulated to complex baseband, the correlator values corresponding to each observed GNSS signal were processed to estimates of the phase and amplitude perturbations induced by ionospheric activity. Being an open-loop postprocessing scheme, a batch estimation of the amplitude and phase was possible, providing highly accurate and reliable characterization [66]. Therefore, these time series are clean multifrequency dynamic-free ionospheric scintillation amplitude and phase traces. From these estimations of carrier phase and amplitude, traditional measures of scintillation activity were computed, such as S_4 and σ_ϕ .

Fig. 10 shows an example of real scintillation amplitude data for a scintillation event at three different GPS

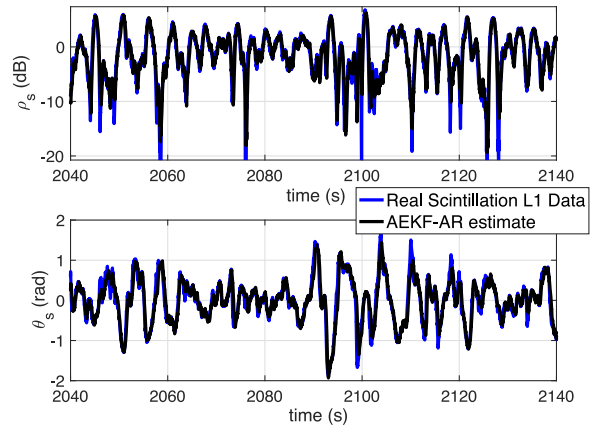


Fig. 11. Real scintillation amplitude and phase data, and the corresponding AEKF-AR estimates for the GPS L1 strong scintillation event #1.

frequency bands. It is clear that it is a strong scintillation scenario because the signal experiences fadings as deep as -30 dB, and the number of fadings below -10 dB is very high.

2) *Dynamics-Free Scintillation Tracking*: First, to verify the correctness of the proposed AR model using real data, we test the scintillation tracking capabilities of the new AEKF-AR in a static scenario directly using the JRC ionospheric scintillation time series (i.e., where phase variations due to dynamics are removed using the multifrequency open-loop postprocessing) for three different scintillation events at different GPS frequency bands. Notice that we use one portion of the real scintillation time series for AR model fitting, and then process the rest of the real traces to obtain the performance results. Fig. 11 plots an example of both real scintillation components and the corresponding AEKF-AR estimates for the GPS L1 strong scintillation event #1. It is clear that the filter is able to correctly track the scintillation amplitude and phase, showing that the AR scintillation model considered in Section III is a valid approach within the KF framework.

Fig. 12 shows the S_4 scintillation indices for the three different scintillation events considered in this section. Events #1 and #2 are severe scintillation scenarios, and event #3 is a moderate to strong scintillation case. Therefore, considering these sets of data we are covering different scintillation conditions. The AEKF-AR scintillation tracking performance for these events is given in Table V. Scintillation amplitude and phase estimation RMSE, named E_{ρ_s} (lineal amplitude dimension) and E_{θ_s} (in rad), respectively, are computed over sequences of 600 s of data. Again, the low estimation error, using sequences of real scintillation data at different frequency bands and for different scintillation events, supports the use of the AR model approximation as a valid approach.

To further justify the correct AR model order, we show the PAF results for real ionospheric scintillation data in Figs. 13 and 14, corresponding to scintillation amplitude and phase, respectively.

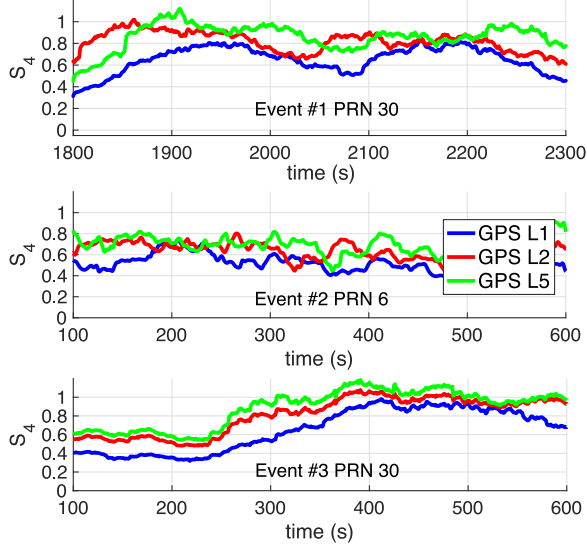


Fig. 12. Real scintillation data S_4 indices for three different scintillation events.

TABLE V
Relative Amplitude and Phase Tracking Error for Real Data Using the AEKF-AR at Different GPS Frequency Bands

Event	E_{ρ_s} L1	E_{θ_s} L1	E_{ρ_s} L2	E_{θ_s} L2	E_{ρ_s} L5	E_{θ_s} L5
#1	0.0178	0.0261	0.0196	0.0303	0.0179	0.0300
#2	0.0174	0.0202	0.0200	0.0241	0.0176	0.0188
#3	0.0204	0.0356	0.0249	0.0721	0.0321	0.1099

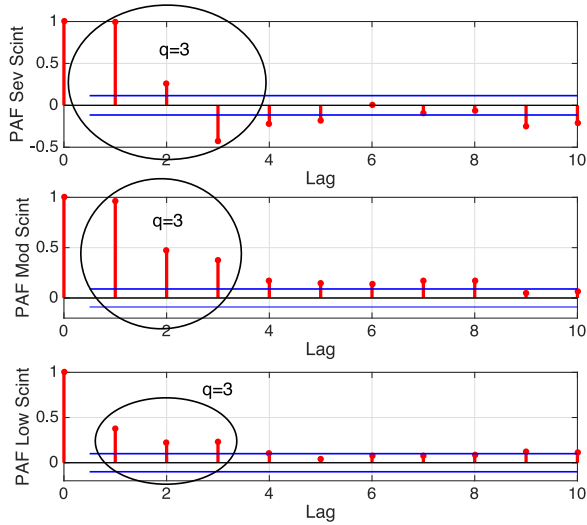


Fig. 13. Sample PAF for real scintillation data model order selection. Severe (top), moderate (middle), and low (bottom) real amplitude scintillation.

3) *New AEKF-AR Performance Using Real Data:* To conclude, we consider again the aeronautical user case with a rapidly varying third-order Doppler profile (acceleration = 20 m/s^2) described at the beginning of the section. That is, we use the JRC real ionospheric scintillation multifrequency amplitude and phase traces, on top of the desired dynamics generated using the SSM described in Section IV.

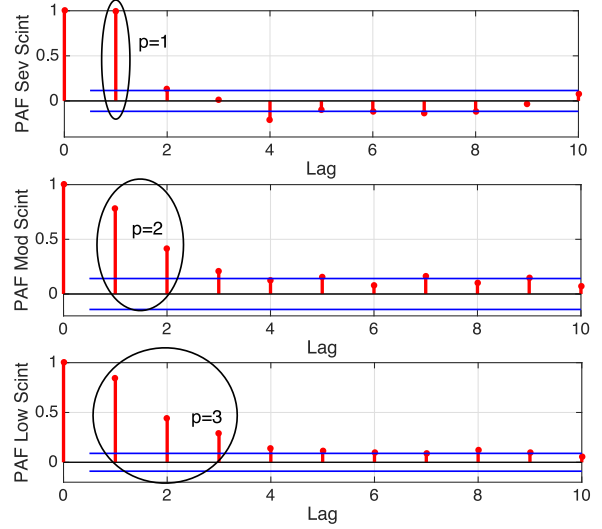


Fig. 14. Sample PAF for real scintillation data model order selection. Severe (top), moderate (middle), and low (bottom) real phase scintillation.

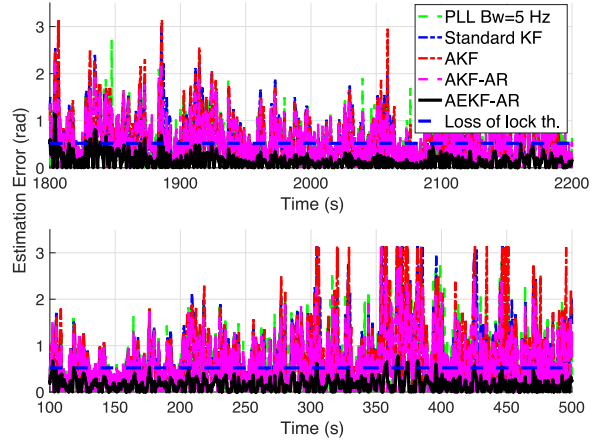


Fig. 15. Estimation error (rad) for the severe scintillation event #1 at GPS L1 (top), and the moderate to strong scintillation event #3 at GPS L2 (bottom).

As in the previous analysis using realistic synthetic CSM data (Cases I–IV in Section VI), the main goal is to obtain the best estimate of the phase related to the user dynamics $\theta_{d,k}$. The dynamics phase estimation RMSE is named E_{θ_s} (rad).

First, to graphically show the performance of the AEKF-AR with respect to the other SoTA methods, we plot in Fig. 15 the estimation error for the severe scintillation event #1 at GPS L1, and the moderate to strong scintillation event #3 at GPS L2. The new AEKF-AR is the only method effectively decoupling both phase components and correctly tracking the scintillation phase component. This fact directly impacts on the dynamics' phase estimation, which is clear from the instantaneous estimation error shown in the figure. The AEKF-AR is the only method providing an estimation error below the loss of lock rule of thumb threshold, and therefore, good scintillation mitigation capabilities. The RMSE for the dynamics' phase estimation

TABLE VI
Root Mean Square Phase Tracking Error
Considering Real Scintillation Data at
Different GPS Frequency Bands

Event #1	$E\theta_d$ L1	$E\theta_d$ L2	$E\theta_d$ L5
PLL	0.493	0.568	0.586
KF	0.588	0.664	0.680
AKF	0.598	0.685	0.725
AKF-AR	0.459	0.503	0.531
AEKF-AR	0.162	0.172	0.188
Event #2	$E\theta_d$ L1	$E\theta_d$ L2	$E\theta_d$ L5
PLL	0.12	0.16	0.17
KF	0.128	0.18	0.19
AKF	0.126	0.18	0.189
AKF-AR	0.105	0.135	0.157
AEKF-AR	0.029	0.037	0.054
Event #3	$E\theta_d$ L1	$E\theta_d$ L2	$E\theta_d$ L5
PLL	0.56	0.626	0.654
KF	0.666	0.757	0.78
AKF	0.688	0.771	0.794
AKF-AR	0.529	0.554	0.616
AEKF-AR	0.195	0.18	0.344

for the different methods is shown in Table VI. From these mean error results, it is clear that the new AEKF-AR provides much better performance and scintillation mitigation capabilities than the rest of the methods.

F. Cycle Slip Performance Analysis

For the complete characterization of the new scintillation mitigation methodology, it is necessary to assess its robustness to cycle slips. This is of capital importance for carrier-based positioning techniques such as RTK and PPP, which rely on the integrity of carrier phase measurements.

First, we analyze the robustness to cycle slips of the different methods using realistic synthetic data generated with the CSM. One realization of the phase error for three different scenarios is shown in Fig. 16, namely Case #1: $\{S_4 = 0.5, \tau_0 = 0.4\}$, Case #2: $\{S_4 = 0.7, \tau_0 = 0.3\}$, and Case #3: $\{S_4 = 0.9, \tau_0 = 0.1\}$. In the moderate scintillation case, only the PLL suffers a cycle slip. In both severe scintillation scenarios (i.e., middle and bottom plots in Fig. 16), we can see several cycle slips, and it is clear that the stronger the scintillation intensity, the higher the number of cycle slips. It is worth mentioning that the new AEKF-AR is systematically robust to cycle slips in a variety of scintillation conditions, which confirms its capabilities. To support this statement, we give the mean number of cycle slips over 500 Monte Carlo runs in Table VII, where each run has 500 s of signal. The following three interesting conclusions can be drawn from these results.

1) KF-based schemes are more robust to cycle slips than traditional PLLs, and AKFs adapting the filter parameters are better than the standard KF architectures.

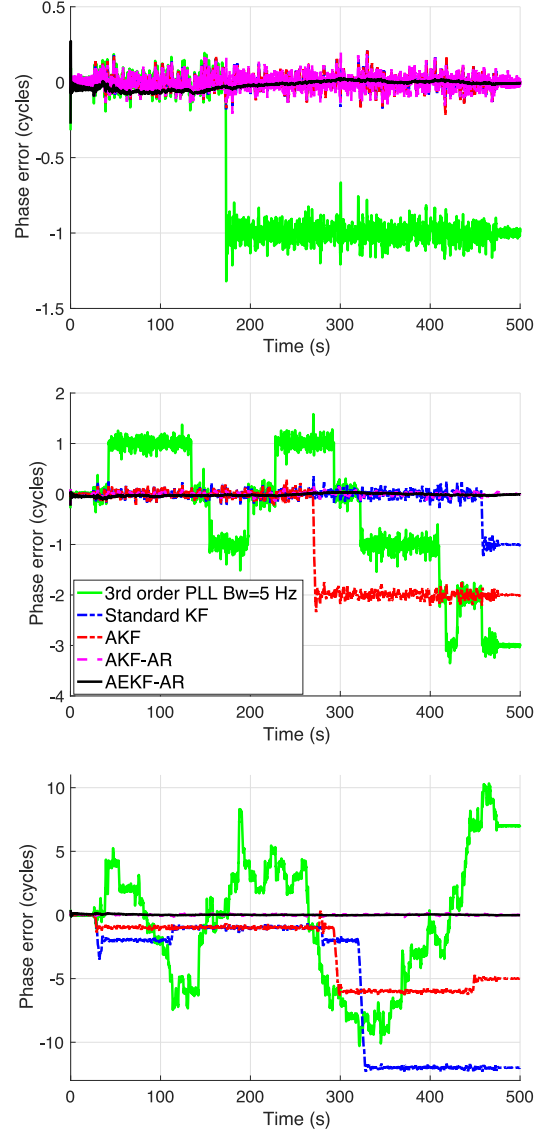


Fig. 16. Phase error for different CSM ionospheric scintillation scenarios: $\{S_4 = 0.5, \tau_0 = 0.5\}$ (top), $\{S_4 = 0.7, \tau_0 = 0.3\}$ (middle), and $\{S_4 = 0.9, \tau_0 = 0.1\}$ (bottom).

TABLE VII
Mean Number of Cycle Slips Over 500
Monte Carlo Runs for Different Scintillation
Scenarios

	Case #1	Case #2	Case #3
PLL	0.476	22.332	407.82
KF	0.006	2.150	216.43
AKF	0	0.532	23.86
AKF-AR	0	0	0.01
AEKF-AR	0	0	0

- 2) Considering the scintillation process into the state-space formulation provides better results than the standard KF-based techniques.
- 3) The AEKF-AR clearly overcomes the limitations of the AKF-AR and the rest of the methods, both in terms of RMSE and cycle slips. No cycle slips were found in 500

TABLE VIII
Number of Cycle Slips for the JRC Real Scintillation Data

	PLL	KF	AKF	AKF-AR	AEKF-AR
Event #1 L1	4	0	2	0	0
Event #1 L2	4	3	3	0	0
Event #1 L5	5	2	4	0	0
Event #2 L1	0	0	0	0	0
Event #2 L2	2	1	0	0	0
Event #2 L5	2	0	0	0	0
Event #3 L1	2	0	1	0	0
Event #3 L2	3	2	2	0	0
Event #3 L5	3	3	2	0	0

iterations (≈ 70 h of data), highlighting its enhanced performance and robustness.

To conclude, we analyze the cycle slip performance for the JRC real ionospheric scintillation data. The results in Table VIII show that while some cycle slips appear with the PLL, KF, and AKF, the scintillation AR SSM formulation improves the filter robustness (i.e., AKF-AR and AEKF-AR), which is in concordance with the results obtained for the CSM data.

VII. CONCLUSION

Ionospheric scintillation effects are known to be a limiting performance factor in advanced GNSS receivers, specifically in receiver architectures that make use of carrier phase measurements for computing position, such as in the case of PPP, RTK, or carrier-based code smoothing techniques. Those approaches, which are now becoming commonplace in mass-market receivers, result in significant improvements in position and velocity accuracy when compared to code delay-based architectures, but they require maintaining uninterrupted carrier phase tracking, avoiding loss of lock. In the presence of scintillation, disturbances in carrier phase measurements can degrade the final receivers performance in terms of position accuracy, and even cause a service blockage. This paper presented a new methodology for efficient scintillation mitigation in advanced GNSS receivers. Together with a SoTA overview, the authors provided an in-depth analysis of the complex random scintillation process approximation. The key step on the new carrier tracking framework is to model both scintillation phase and amplitude as an AR process. Using such approximation, it is possible to embed the undesired scintillation effects into the state-space formulation of the problem, then being capable to keep track of both phase contributions. In spite of its simplicity, this statistical model captures the behavior of such physical phenomenon and exhibits enhanced scintillation mitigation capabilities when compared to SoTA methods based on PLLs or KFs without such augmented state space. The proposed method was put under test both by computer simulations and by using real-life data gathered in a measurement campaign. Results show that the proposed method performs remarkably better in phase tracking than SoTA techniques, reducing cycle slips and effectively decoupling the phase disturbances caused

by scintillation from the carrier-phase dynamics caused by the changing geometry, thus enhancing the availability and accuracy of carrier phase measurements in a GNSS receiver in the presence of ionospheric scintillation events.

REFERENCES

- [1] J. Seo
Overcoming ionospheric scintillation for worldwide GPS aviation
Ph.D. dissertation, Dept. Aeronaut. Astronaut., Stanford Univ., Stanford, CA, USA, Jun. 2010.
- [2] u-blox NEO-M8P
Thalwil, Switzerland. [Online]. Available: <https://www.u-blox.com/en/product/neo-m8p>, Accessed on: Jan. 10, 2017.
- [3] NVS Technologies AG, Montlingen, Switzerland NV08C-RTK. 2015. [Online]. Available: <http://www.nvs-gnss.com/products/receivers/item/39-nv08c-rtk.html>. Accessed on: Jan. 10, 2017.
- [4] A. Somieski, E. Favey, and C. Burgi
Precise point positioning with single-frequency mass market receivers
In *Proc. Inst. Navig. GNSS*, Savannah, GA, USA, Sep. 2008, pp. 1429–1436.
- [5] European Global Navigation Satellite Systems Agency, Prague, Czech Republic CIGALA: Concept for ionospheric-scintillation mitigation for professional GNSS in Latin America
, 2016. [Online]. Available: <http://www.gsa.europa.eu/concept-ionospheric-scintillation-mitigation-professional-gnss-latin-america>. Accessed on: Jan. 19, 2017.
- [6] European Commission, Brussels, Belgium CALIBRA: Countering GNSS high accuracy applications limitation due to ionospheric disturbance in Brazil
, 2016. [Online]. Available: http://cordis.europa.eu/project/rcn/206627_en.html. Accessed on: Jan. 19, 2017.
- [7] European Commission, Brussels, Belgium TRANSMIT: Training research and applications network to support the mitigation of ionospheric threats
, 2014. [Online]. Available: http://cordis.europa.eu/result/rcn/58089_en.html. Accessed on: Jan. 19, 2017.
- [8] R. P. Cerdeira and Y. Béniguel
The MONITOR project: Architecture, data and products
In *Proc. Ionospheric Effects Symp.*, Alexandria, VA, USA, May 2011, pp. 1–6.
- [9] NovAtel Inc., Calgary, AB, Canada GPStation-6 triple-frequency GISTM receiver
, 2004. [Online]. Available: <http://www.novatel.com/products/scintillation-tec-monitor>. Accessed on: Jan. 19, 2017.
- [10] Septentrio, Heverlee, Belgium PolaRxS PRO
, 2015. [Online]. Available: <http://www.septentrio.com/products/gnss-receivers/reference-receivers/polarxs>. Accessed on: Jan. 19, 2017.
- [11] European Commission, Brussels, Belgium MISW: Mitigation of space weather threats to GNSS services
, 2014. [Online]. Available: <http://misw.info/>. Accessed on: Jan. 19, 2017.
- [12] U. Mengali and A. N. D’Andrea
Synchronization Techniques for Digital Receivers. New York, NY, USA: Plenum, 1997.
- [13] E. D. Kaplan, Ed.
Understanding GPS: Principles and Applications, 2nd ed. Norwood, MA, USA: Artech House, 2006.
- [14] J. Vilà-Valls, P. Closas, C. Fernández-Prades, J. A. López-Salcedo, and G. Seco-Granados
Adaptive GNSS carrier tracking under ionospheric scintillation: Estimation vs mitigation
IEEE Commun. Lett., vol. 19, no. 6, pp. 961–964, Jun. 2015.

- [15] J. Vilà-Valls, P. Closas, and C. Fernández-Prades
Advanced KF-based methods for GNSS carrier tracking and ionospheric scintillation mitigation
In *Proc. IEEE Aerosp. Conf.*, Big Sky, MN, USA, Mar. 2015, pp. 1–10, doi: [10.1109/AERO.2015.7118930](https://doi.org/10.1109/AERO.2015.7118930).
- [16] T. E. Humphreys *et al.*
GPS carrier tracking loop performance in the presence of ionospheric scintillations
In *Proc. Inst. Navig. GNSS*, Long Beach, CA, USA, Sep. 2005, pp. 156–167.
- [17] W. Yu, G. Lachapelle, and S. Skone
PLL performance for signals in the presence of thermal noise, phase noise, and ionospheric scintillation
In *Proc. Inst. Navig. GNSS*, Fort Worth, TX, USA, Sep. 2006, pp. 1341–1357.
- [18] L. Zhang and Y. T. Morton
Tracking GPS signals under ionosphere scintillation conditions
In *Proc. Inst. Navig. GNSS*, Savannah, GA, USA, Sep. 2009, pp. 227–234.
- [19] G. Skone, G. Lachapelle, D. Yao, W. Yu, and R. Watson
Investigating the impact of ionospheric scintillation using a GPS software receiver
In *Proc. Inst. Navig. GNSS*, Long Beach, CA, USA, Sep. 2005, pp. 1126–1137.
- [20] R. Tiwari, S. Skone, S. Tiwari, and H. J. Strangeways
WBMod assisted PLL GPS software receiver for mitigating scintillation affect in high latitude region
In *Proc. 30th URSI Gen. Assem. Sci. Symp.*, Istanbul, Turkey, Aug. 2011, pp. 1–4, doi: [10.1109/URSIGASS.2011.6050861](https://doi.org/10.1109/URSIGASS.2011.6050861).
- [21] T.-Y. Chiou, D. Gebre-Egziaber, T. Walter, and P. Enge
Model analysis on the performance for an inertial aided FLL-assisted PLL carrier tracking loop in the presence of ionospheric scintillation
In *Proc. Inst. Navig., Nat. Tech. Meeting*, San Diego, CA, USA, vol. 2, Jan. 2007, pp. 1276–1295.
- [22] T.-Y. Chiou, J. Seo, T. Walter, and P. Enge
Performance of doppler-aided GPS navigation system for aviation applications under ionospheric scintillation
In *Proc. Inst. Navig. GNSS*, Savannah, GA, USA, Sep. 2008, pp. 1139–1147.
- [23] T.-Y. Chiou
Design of a Doppler-aided GPS navigation system for weak signals caused by strong ionospheric scintillation
Ph.D. dissertation, Dept. Aeronaut. Astronaut., Stanford Univ., Stanford, CA, USA, May 2010.
- [24] X. Mao, Y. T. Morton, L. Zhang, and Y. Kou
GPS carrier signal parameters estimation under ionospheric scintillation
In *Proc. Inst. Navig. GNSS*, Portland, OR, USA, Sep. 2010, pp. 3277–3283.
- [25] S. Fantinato, D. Rovelli, and P. Crosta
The switching carrier tracking loop under severe ionospheric scintillation
In *Proc. Navig. Technol.*, Noordwijk, The Netherlands, Dec. 2012, pp. 1–6, doi: [10.1109/NAVITEC.2012.6423056](https://doi.org/10.1109/NAVITEC.2012.6423056).
- [26] N. Kassabian and Y. J. Morton
Extending integration time for Galileo tracking robustness under ionosphere scintillation
In *Proc. IEEE/ION Position, Location Navig. Symp.*, Monterey, CA, USA, May 2014, pp. 59–72.
- [27] J. López-Salcedo, J. Peral-Rosado, and G. Seco-Granados
Survey on robust carrier tracking techniques
IEEE Commun. Surveys Tuts., vol. 16, no. 2, pp. 670–688, Apr. 2014.
- [28] M. L. Psiaki *et al.*
Tracking L1 C/A and L2C signals through ionospheric scintillations
In *Proc. Inst. Navig. GNSS*, Fort Worth, TX, USA, Sep. 2007, pp. 246–268.
- [29] C. Macabiau *et al.*
Kalman filter based robust GNSS signal tracking algorithm in presence of ionospheric scintillations
In *Proc. Inst. Navig. GNSS*, Nashville, TN, USA, Sep. 2012, pp. 3420–3434.
- [30] V. Barreau *et al.*
Kalman filter based robust GNSS signal tracking algorithm in presence of ionospheric scintillations
In *Proc. ESA Navig. Technol.*, Noordwijk, The Netherlands, Dec. 2012, pp. 2325–5439.
- [31] L. Zhang, Y. T. Morton, F. Van Graas, and T. Beach
Characterization of GNSS signal parameters under ionosphere scintillation conditions using software-based tracking algorithms
In *Proc. IEEE/ION Position, Location Navig. Symp.*, Indian Wells, CA, USA, May 2010, pp. 264–275.
- [32] Y.-H. Chen, J.-C. Juang, and T.-L. Kao
Robust GNSS signal tracking against scintillation effects: A particle filter based software receiver approach
In *Proc. Int. Tech. Meeting Inst. Navig.*, San Diego, CA, USA, Jan. 25–27, 2010, pp. 627–635.
- [33] J. Vilà-Valls, P. Closas, and C. Fernández-Prades
On the identifiability of noise statistics and adaptive KF design for robust GNSS carrier tracking
In *Proc. IEEE Aerosp. Conf.*, Big Sky, MN, USA, Mar. 2015, pp. 1–10, doi: [10.1109/AERO.2015.7118929](https://doi.org/10.1109/AERO.2015.7118929).
- [34] L. Zhang, Y. T. Morton, and M. M. Miller
A variable gain adaptive Kalman filter-based GPS carrier tracking algorithms for ionosphere scintillation signals
In *Proc. Int. Tech. Meeting Inst. Navig.*, San Diego, CA, USA, 2010, pp. 3107–3114.
- [35] J.-H. Won, B. Eissfeller, T. Pany, and J. Winkel
Advanced signal processing scheme for GNSS receivers under ionospheric scintillation
In *Proc. IEEE/ION Position, Location Navig. Symp.*, Myrtle Beach, SC, USA, Apr. 2012, pp. 44–49.
- [36] J. H. Won
A novel adaptive digital phase-lock-loop for modern digital GNSS receivers
IEEE Commun. Lett., vol. 18, no. 1, pp. 46–49, Jan. 2014.
- [37] M. Susi *et al.*
Design of a robust receiver architecture for scintillation monitoring
In *Proc. IEEE Position, Location Navig. Symp.*, Monterey, CA, USA, May 2014, pp. 73–81.
- [38] M. Susi, M. Andreotti, and M. Aquino
Kalman filter based PLL robust against ionospheric scintillation
In *Mitigation of Ionospheric Threats to GNSS: An Appraisal of the Scientific and Technological Outputs of the TRANSMIT Project*, R. Notarpietro, Ed. Rijeka, Croatia: InTech, 2014, pp. 23–36.
- [39] J. Vilà-Valls, J. A. López-Salcedo, and G. Seco-Granados
An interactive multiple model approach for robust GNSS carrier phase tracking under scintillation conditions
In *Proc. IEEE Int. Conf. Acoust., Speech, Signal Process.*, Vancouver, BC, Canada, May 2013, pp. 6392–6396.
- [40] S. Peng
A multi-constellation multi-frequency GNSS software receiver design for ionosphere scintillation studies
Ph.D. dissertation, Virginia Polytech. Inst. State Univ., Blacksburg, VA, USA, Jul. 2012.
- [41] T. Lin, G. Lachapelle, and L. P. Souto Fortes
How do modern GNSS signal processing techniques deal with equatorial ionospheric scintillation
Inside GNSS, vol. 9, no. 1, pp. 26–34, Jan./Feb. 2014.
- [42] M. Aquino *et al.*
Towards forecasting and mitigating ionospheric scintillation effects on GNSS
In *Proc. ELMAR*, Zadar, Croatia, Sep. 2007, pp. 63–67, doi: [10.1109/ELMAR.2007.4418801](https://doi.org/10.1109/ELMAR.2007.4418801).

- [43] R. Warnant *et al.*
Mitigation of ionospheric effects on GNSS
Ann. Geophys., vol. 52, no. 3, pp. 373–390, Jun./Aug. 2009.
- [44] H. J. Strangeways and R. Tiwari
Prediction and mitigation of ionospheric scintillation and tracking jitter for GNSS positioning
In *Proc. ELMAR*, Zadar, Croatia, Sep. 2013, pp. 319–322.
- [45] P. Henkel, K. Giger, and C. Gunther
Multifrequency, multisatellite vector phase-locked loop for robust carrier tracking
IEEE J. Sel. Topics Signal Process., vol. 3, no. 4, pp. 674–681, Aug. 2009.
- [46] L. Deambrogio and C. Macabiau
Vector tracking aiding for carrier phase estimation in the presence of ionospheric scintillation
In *Proc. Int. Tech. Meeting Inst. Navig.*, San Diego, CA, USA, Jan. 2013, pp. 333–342.
- [47] F. M. G. Sousa and F. D. Nunes
Performance analysis of a VDFLL GNSS receiver architecture under ionospheric scintillation and multipath conditions
In *Proc. IEEE/ION Position, Location Navig. Symp.*, Monterey, CA, USA, May 2014, pp. 602–611.
- [48] M. Najmafshar, F. Ghafoori, and S. Skone
Robust receiver design for equatorial regions during solar maximum
In *Proc. Inst. Navig. GNSS+*, Nashville, TN, USA, Sep. 2013, pp. 3255–3262.
- [49] J. Seo and T. Walter
Future dual-frequency GPS navigation system for intelligent air transportation under strong ionospheric scintillation
IEEE Trans. Intell. Transp. Syst., vol. 15, no. 5, pp. 2224–2236, Oct. 2014.
- [50] M. Carrol, Y. J. Morton, and E. Vinande
Triple frequency GPS signal tracking during strong ionospheric scintillation over Ascension Island
In *Proc. IEEE/ION Position, Location Navig. Symp.*, Monterey, CA, USA, May 2014, pp. 43–49.
- [51] P. M. Kintner, T. E. Humphreys, and J. Hinks
GNSS and ionospheric scintillation: How to survive the next solar maximum
Inside GNSS, vol. 4, no. 4, pp. 22–33, Jul./Aug. 2009.
- [52] T. E. Humphreys, M. L. Psiaki, and P. M. Kintner
Modeling the effects of ionospheric scintillation on GPS carrier phase tracking
IEEE Trans. Aerosp. Electron. Syst., vol. 46, no. 4, pp. 1624–1637, Oct. 2010.
- [53] J. Secan, R. Bussey, and E. Fremouw
High-latitude upgrade to the wideband ionospheric scintillation
Radio Sci., vol. 32, no. 4, pp. 1567–1574, Jul./Aug. 1997.
- [54] ITU Ionospheric propagation data and prediction methods required for the design of satellite services and systems
Int. Telecommun. Union, Geneva, Switzerland, Tech. Rep. ITU-R P.531–12, Sep. 2013.
- [55] T. E. Humphreys, M. L. Psiaki, J. C. Hinks, B. O’Hanlon, and P. M. Kintner
Simulating ionosphere-induced scintillation for testing GPS receiver phase tracking loops
IEEE J. Sel. Topics Signal Process., vol. 3, no. 4, pp. 707–715, Aug. 2009.
- [56] S. M. Kay
Fundamentals of Statistical Signal Processing: Estimation Theory. Englewood Cliffs, NJ, USA: Prentice-Hall, 1993.
- [57] J. J. Spilker
Fundamentals of signal tracking theory
In *Global Positioning System: Theory and Applications*, vol. 1, B. W. Parkinson and J. J. Spilker, Eds. Washington, DC, USA: Amer. Inst. Aeronaut. Astronaut., 1996, pp. 245–328.
- [58] V. P. Ipatov
Spread Spectrum and CDMA: Principles and Applications. New York, NY, USA: Wiley, 2005.
- [59] A. Papatoutian
On phase-locked loops and Kalman filters
IEEE Trans. Commun., vol. 47, no. 5, pp. 670–672, May 1999.
- [60] H. Shu, E. P. Simon, and L. Ros
Third-order Kalman filter: Tuning and steady-state performance
IEEE Signal Process. Lett., vol. 20, no. 11, pp. 1082–1085, Nov. 2013.
- [61] J. Vilà-Valls, P. Closas, M. Navarro, and C. Fernández-Prades
Are PLLs dead? A tutorial on Kalman filter-based techniques for digital carrier synchronization
IEEE Aerosp. Electron. Syst. Mag., vol. 32, no. 7, pp. 28–45, Jul. 2017.
- [62] B. Anderson and J. B. Moore
Optimal Filtering. Englewood Cliffs, NJ, USA: Prentice-Hall, 1979.
- [63] J. T. Curran
Enhancing weak-signal carrier phase tracking in GNSS receivers
Int. J. Navig. Observ., vol. 2015, Sep. 2015, Art. no. 295029, doi: [10.1155/2015/295029](https://doi.org/10.1155/2015/295029).
- [64] J. H. Won
A tuning method based on signal-to-noise power ratio for adaptive PLL and its relationship with equivalent noise bandwidth
IEEE Commun. Lett., vol. 17, no. 2, pp. 393–396, Feb. 2013.
- [65] A. J. Van Dierendonck, J. Klobuchar, and Q. Hua
Ionospheric scintillation monitoring using commercial single frequency C/A code receivers
In *Proc. Int. Tech. Meeting Inst. Navig. GPS*, Salt Lake City, UT, USA, Sep. 1993, pp. 1333–1342.
- [66] J. T. Curran, M. Bavaro, A. Morrison, and J. Fortuny
Operating a network of multi-frequency software-defined ionosphere monitoring receivers
In *Proc. Inst. Navig. GNSS+*, Tampa, FL, USA, Sep. 2015, pp. 44–49.
- [67] J. T. Curran, M. Bavaro, A. Morrison, and J. Fortuny
Event identification & recording for scintillation monitoring stations
In *Proc. Int. Tech. Meeting Inst. Navig.*, Dana Point, CA, USA, Sep. 2015, pp. 114–122.



Jordi Vilà-Valls (SM'17) received the Ph.D. degree in electrical engineering (signal processing) from Grenoble Institute of Technology, Grenoble, France, in 2010.

He is currently a Researcher with the Statistical Inference for Communications and Positioning Department, Centre Tecnològic de Telecomunicacions de Catalunya (CTTC/CERCA), Barcelona, Spain. His research interests include statistical signal processing at large, nonlinear Bayesian inference, robust filtering and adaptive signal processing methods, with applications to GNSS, positioning and tracking systems, wireless communications, and aerospace science.



Pau Closas (S'04–M'10–SM'13) received the M.S. and Ph.D. degrees in electrical engineering and the M.S. degree in advanced mathematics and mathematical engineering from the Universitat Politècnica de Catalunya, Barcelona, Spain, in 2003, 2009, and 2014, respectively.

He is currently an Assistant Professor with the Department of Electrical and Computer Engineering, Northeastern University, Boston, MA, USA. His research interests include statistical signal processing and robust stochastic filtering, with applications to GNSS, positioning and tracking systems, wireless communications, and mathematical biology.

Dr. Closas was the recipient of the EURASIP Best Ph.D. Thesis Award 2014, the 9th Duran Farell Award for Technology Research, and the 2016 ION Early Achievement Award.



Carles Fernández-Prades (S'02–M'06–SM'12) received the Ph.D. degree in electrical engineering from Universitat Politècnica de Catalunya, Barcelona, Spain, in 2006.

He is currently the Senior Researcher and the Head of the Statistical Inference for Communications and Positioning Department, Centre Tecnològic de Telecomunicacions de Catalunya (CTTC/CERCA), Barcelona, Spain, where he previously was the Head of the Communication Subsystems Area (2006–2013) and the Head of the Communications Systems Division (2013–2016). His research interests include statistical and multisensor signal processing, estimation and detection theory, and Bayesian filtering, with applications related to communication systems, GNSS, and software-defined radio technology.



James Thomas Curran (M'10) received Ph.D. degree in telecommunications from the Department of Electrical Engineering, University College Cork, Cork, U.K., in 2010.

He is currently a Radionavigation Engineer with the European Space Agency, Noordwijk, The Netherlands. He was a Researcher with the University of Calgary and the Joint Research Center of the European Commission focusing on security and radionavigation. His research interests include software-defined radio, information theory, signal processing, and cryptography.